Thiahelicene-grafted halloysite nanotubes: Characterization, biological studies and pH triggered release

Thiahelicene-grafted halloysite nanotubes: characterization, biological studies and pH triggered release

Tommaso Taroni[1,2], Silvia Cauteruccio[1,*], Riccardo Vago[3], Stefano Franchi[4], Emanuela Licandro[1], Silvia Ardizzone[1,2] and Daniela Meroni[1,2,*]

a. Department of Chemistry, Università degli Studi di Milano, Via Golgi 19, 20133, Milan, Italy. Email: daniela.meroni@unimi.it; silvia.cauteruccio@unimi.it

b. Consorzio INSTM, Via Giusti 9, 50121, Florence, Italy

c. Urological Research Institute, Ospedale San Raffaele, 20132, Milan, Italy

d. Elettra-Sincrotrone Trieste, 34149 Basovizza, Trieste, Italy

Abstract

A drug delivery nanosystem was designed linking DNA intercalating thiahelicenes to halloysite nanotubes. Imine chemistry was adopted to attach and release the active principle in acidic environments like those surrounding tumoral cells. Spectrophotometric analyses, release kinetics and in vitro tests on two cell lines confirm the potential of this novel nanoconstruct.

Helicenes are polycyclic compounds in which ortho-condensed (hetero)aromatic rings adopt a helical conformation to avoid the overlapping of the terminal rings. Due to their nonplanar π-electron structure, such molecules are inherently chiral and exhibit unique structural and chiroptical properties that have stimulated studies in numerous fields.1 Among them, the similarity of helicenes to chiral helical structures found in natural biomolecules, such as DNA and α-helix secondary structures of proteins, has promoted research in biochemistry,2 including studies on potential applications as DNA intercalators,3 as fluorescent dyes for bioimaging,4 and as inhibitors of telomerase.5 In this respect, the loading of helicene derivatives on nanocarrier systems can enable a more precise localization and targeted delivery of the molecule. However, nanosystems containing helicene derivatives have been scarcely investigated so far, and most of these studies are focused on the use of gold,6, 7 silica8 and organic nanoparticles (NPs). Recently, some of us have reported the intracellular delivery of a luminescent tetrathia[7]helicene (7-TH) mediated via PLGA NPs.8 Organic NPs based on fluorescent tetrahydro[5]helicene9 and squalene-based nanoassemblies containing diaza[4]helicene dyes have also been investigated for cell fluorescence imaging.10 In these reports, the loading is either driven by physical interactions, leading to poor control over the release process, or it is based on stable covalent bonds such as amide bonds or Au-S interactions with thiol groups. To the best of the authors' knowledge, no triggered release investigations have been reported.

In the present work, a thiahelicene derivative was grafted on a nanostructured system never previously investigated with helicene-derivatives: halloysite nanotubes (HNT). Halloysite is an aluminosilicate clay, with the raw formula Al2(OH)4Si2O5·nH2O,11 which is naturally extracted in the form of nanotubes exposing

siloxane/silanol groups on the outer surface and aluminium hydroxide groups on the inner lumen.12 This chemical duality enables the selective functionalization of the two surfaces.13, 14 Thanks to their availability, good biocompatibility and low cost, halloysite nanotubes have proved promising candidates for a series of applications, including diagnostic probes and drug delivery systems.15 Here we designed and prepared a novel nanoconstruct based on HNT in which the tetrathiahelicene-based aldehyde (±)-7-THA,16 in the form of a racemic mixture for this preliminary study, is covalently linked to the oxide carrier. Acid responsiveness is one of the most studied means to elicit the triggered release of a bioactive component,17 as it is known that acidic extracellular pH is a major feature of tumour tissue.18 For this reason, we designed a pH-sensitive drug delivery system based on imine chemistry (Scheme 1). Indeed, the imine bond is a suitable tool to achieve the pH triggered release of biomolecules, which can be integrated in bioorthogonal systems.19 To this purpose, we reacted (±) 7-THA with HNT covered with amino groups from (3-aminopropyl)triethoxysilane (APTES), and then tested the reversibility of this bond under different pH conditions, to measure the relative release efficiency of 7 TH.

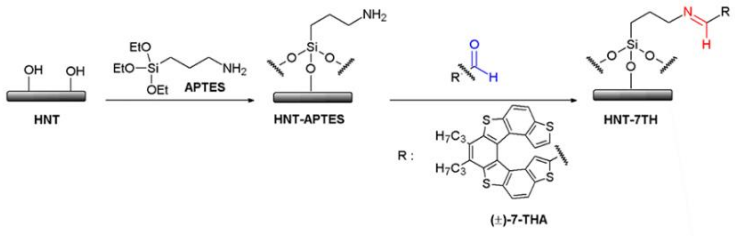

Scheme 1 Reaction pathway for the preparation of HNT-7TH.

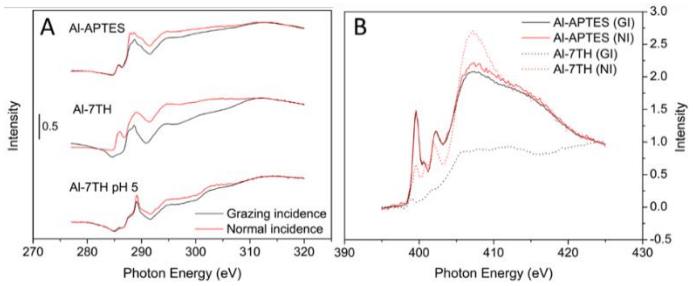

Fig. 1 C K-edge (A) and N K-edge (B) NEXAFS spectra of the functionalized Al films.

In this first study, commercial HNT from iMinerals Inc. was used, as received. Diffractograms show halloysite as the main phase, with kaolinite and minor quartz impurities (Figure S1).

Table 1 Surface atomic percentage amounts of the various samples, obtained by XPS.

Element	HNT	HNT-APTES	HNT-7TH	HNT-7TH pH 5
Al	11.9	7.9	5.7	2.7
Si	14.8	13.3	9.7	5.9
S	-	-	3.3	0.6
C	16.6	36.9	50.7	59.1
N	-	3.5	3.2	1.9
O	56.7	38.4	27.4	29.8

The pristine HNT has a specific surface area of 33.7 $m^2 g^{-1}$, with a total pore volume of 0.204 mL g^{-1}. This is mostly represented by the inner lumen of the nanotubes, as the pores with a diameter of 20-80 nm account for around 60% of the total pore volume. Functionalization was carried out by heating a suspension of HNT with APTES in anhydrous conditions, as reported in section 1.1 of the Electronic Supplementary Information. Later, 7-THA was grafted on the surface following the procedure reported in section 1.2 of the ESI.

The loading of the nanosystem was 0.9%w for HNT-APTES and 3.5%w for HNT-7-TH, as estimated by TGA analyses. By correlating these results with the specific surface area of pristine HNT, a rough estimate of the molecule surface coverage, δ can be obtained. As APTES possesses three ethoxy moieties, during condensation it can form a variable number of bonds (from 1 to 3) with the oxide surface or neighbouring APTES molecules;[20] hence, knowing exactly what is the molecular weight to consider during thermal degradation is rather difficult.[21] In the present case, the δ value of HNT-APTES can thus range from 1.2 to 3.1 molecules/nm^2 depending on whether a single bond formation or a full condensation are assumed, averaging at 2 molecules/nm^2: these values compare well with literature data concerning APTES monolayers on glass and silicon substrates (2.1-4.2 molecules/nm^2).[22, 23] The δ value for 7-TH is estimated to be slightly lower (1.3 molecules/nm^2). Since the calculated co-area for standing and lying 7-TH molecules is about 0.6 nm^2 and 1.25 nm^2 respectively,[24] the δ value supports an average vertical orientation of the helicene moieties at the surface, as confirmed by the NEXAFS spectra (*vide infra*).

After functionalization, HNT-7TH was treated in mild acidic conditions in order to elicit the release of the 7TH moiety, as reported in the ESI, section 3.1: XPS analyses were carried out at each stage of the whole preparation process of HNT-7TH and after the release test at pH 5, to monitor the presence and release of adsorbates on the surface. Results are summarized in Table 1. As expected, the pristine HNT surface is characterized by the presence of Al, Si and O, together with some adventitious C (Figure S2a). Binding energies of Al (74.9 and 76.2 eV) and Si (103.1 and 104.4 eV) peaks are in line with the literature,[25] and could be attributed to M-O and M-OH groups, respectively. Although the stoichiometric ratio between Al and Si should be 1:1, the latter appears to be more abundant, due to attenuation of the inner layer signal.[26]

After APTES functionalization a few changes can be noticed: the Si signal presents a lower energy peak at 102.0 eV (Figure S2b), which can be attributed to the siloxanes from APTES,[20] while the bulk SiO_2 component

at 103.1 becomes attenuated.[27] The carbon content increases due to the carbon chains of the organic molecule. Moreover, a broad N signal becomes appreciable (Figure S3) in agreement with the literature, showing for APTES-modified oxides the occurrence of two peak components relative to free and hydrogen-bonded NH_2.[20] The N/Si atomic ratio is 0.26, suggesting the presence of 1 APTES molecule every 3 surface Si atoms. Based on halloysite structure calculations (9 Si atoms/nm^2),[28] we can conclude that the APTES molecular density δ is around 3 molecules/nm^2, which is actually within the range extracted from TGA, supporting a fully condensed APTES layer.

Relatively to HNT-APTES, HNT-7TH shows a further C increase. Additionally, the two peaks of S 2p are appreciable (Figure S2c): the binding energy of the $2p_{3/2}$ component (163.8 eV) is attributable to the thiophenes in the tetrathiahelicene scaffold,[29] indicating that 7-TH was successfully bound to the surface. Slight changes can also be noticed in the shape of the N signal: after functionalization with 7-THA, the shape of the peak changes, highlighting an increase in the component at lower binding energy. The latter could be related to the formation of an imine C=N bond, since its signal coincides with that of free NH_2.[30, 31]

After 48 h of treatment at pH 5, the amount of S appears greatly reduced: the S : N atomic ratio for HNT-7TH upon treatment goes from 1.03 to 0.33, indicating a loss of almost 70% of the loaded molecule. The carbon and oxygen amounts increase, due to the adsorption of citrate species present in the buffer solution used for the release test, attenuating the N 1s signal. The latter becomes more similar to the HNT-APTES sample, indicating the breaking of the imine bond. Furthermore, the presence of a charged species such as citrate ions might favour the NH_3^+ form of APTES, possibly explaining the slight increase in its component in the N 1s signal, as shown in Figure S2.

To further investigate the surface reactivity of bonded 7-TH, the molecular orientation of the functionalizing moieties at the oxide surface was also investigated via angle-resolved near-edge X-ray absorption fine structure (NEXAFS) spectroscopy. For this purpose, as models of the HNT surface, AlO(OH) and SiO_2 films were prepared, functionalized with 7-TH and subjected to the same treatment at pH 5 for 48 h. As APTES functionalization is not selective towards either one of the surfaces of halloysite, in this paper we will mainly refer to the inner alumina layer, as the binding in the inner lumen leads to a more controlled release.

C K-edge and N K-edge NEXAFS spectra of the bare and functionalized films were collected at grazing and normal incidence (Figure 1). With respect to our previous study on APTES-functionalized TiO_2,[20] no preferential orientation of the alkyl chains was found in the presently investigated APTES-functionalized oxide films, supporting the formation of a disorganized organic layer. On the contrary, upon reaction with the helicene derivative, preferential orientation of the organic molecules was observed for both sets of substrates: in particular, the C 1s → π*(C=C, C=N) component at 286.0 eV, related to the conjugated ring structure,[32] and the N 1s → π*(N=C) and N 1s → σ*(N—C)[31] components at 399.6 eV and 407.2 eV, respectively, suggested a preferential orientation of the aromatic rings of helicene normal to the oxide surface, possibly as a result of π-π stacking interactions. This occurrence may prove useful to promote drug

loading. Interestingly, after treatment in mild acidic conditions, NEXAFS spectra show no preferential orientation of the organic chains; furthermore, the C 1s → π*(C=C, C=N) transitions become negligible, while a component appears at 289.2 eV in C K-edge spectra, which can be attributed to the 1s → π*(C=O) transition[33] of the citrate anions from the buffer solution, possibly interacting with the protonated amine group formed upon the breaking of the imine bond. Fully comparable results have been obtained for the SiO_2 film.

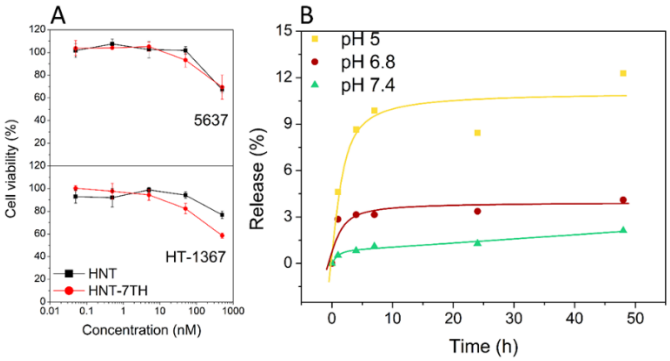

Fig. 2 Cell viability assay on 5637 and HT-1367 cell lines (A) and BDT release kinetics measured over 48 h (B).

We tested the effect of HNT-APTES or HNT-7TH on the viability of bladder cancer cells. To address tumour heterogeneity, we used two different cell lines, named 5637 and HT-1376, which differ in grading, proliferation rate and metabolism, with the latter more prone to acidifying the culture medium. We assessed cell viability by incubating cells with serial logarithmic dilutions of HNT-APTES or HNT-7TH ranking from 0.5 μM to 0.05 nM for 72 h and then a MTT viability assay was performed (Figure 2a). HNT-APTES were slightly toxic for cells at the highest tested concentrations in both the cell models. HNT-7TH showed overlapping activity with HNT-APTES on 5637 cells, while it was found to be significantly more active on HT-1376. This result is in line with the acidification propensity of the two cell lines: at the end of the experiment, 5637 culture medium had pH 7.2, while HT-1376 medium was more acidic with pH 6.8. In fact, 7-TH is expected to be more released from the HNT at slightly acidic pH, as demonstrated by *in vitro* assays, by the breakdown of the imine bond. The free 7-TH was likely to interact with DNA of HT-1376 causing a reduction of cell viability. This was not the case in 5637 cells, due to the pH of the culture medium, not compatible with 7-TH release. This approach can be valuable in the tumours that show a strong metabolic rewiring by stimulating the “aerobic glycolysis”, instead of respiration, with the concomitant production and secretion of lactate. Since it was confirmed that 7-TH was successfully loaded and released from HNT, further studies on the release kinetics and their dependence on environmental pH were performed. Tests were carried out on a more water-soluble mimic, benzo[1,2-*b*:4,3-*b*’]dithiophene (BDT), which represents a suitable portion of 7-TH. Its formyl derivative,[34] from a reactivity point of view, is expected to behave very similarly to 7-TH. As reported in section 3.1 of the ESI, release tests were performed by suspending HNT-7TH in three different

buffer solutions, and monitoring the release for 48 h. Figure 2b reports the results of these tests as release percentage against time. Release efficiency was highest for the treatment at pH 5, reaching maximum BDT solubility after only 7 h. On the contrary, release is much slower in the case of higher pH: at pH 7.4 the amount of released BDT is negligible even after 48 h, while decreasing the pH value by just 0.6 units to 6.8 visibly increases release rates. Furthermore, FTIR spectroscopy was performed on HNT-BDT before and after release at pH 5, 6.8 and 7.4. We report the differential spectra with respect to HNT-APTES, between 1800 and 1400 cm^{-1} (Figure S4). The main feature of the HNT-BDT spectrum is the peak at 1632 cm^{-1}, which can be attributed to the imine bond, formed upon the reaction between APTES NH_2 groups and BDT. Upon release tests, other features become appreciable: the sample treated at pH 5 shows strong and broad signals due to the presence of citrate, obscuring other signals. For samples treated at pH 7.4 and 6.8 both the imine signal and the water bending mode at 1650 cm^{-1} are appreciable, with different relative intensities. As can be seen, the relative intensity of the two peaks gets closer when decreasing the release pH, suggesting that there is less imine on the surface, thus supporting the breaking of the imine bond: at pH 7.4 the peaks are very similar to the untreated sample, whereas at 6.8 their intensities are fully comparable. These results support those obtained through *in vitro* studies, which suggested that a small difference in cellular environment pH could be responsible for the higher cytotoxicity registered.

In conclusion, we developed a novel nanosystem where thiahelicene is grafted via an imine bond to halloysite. The success of the adopted functionalization approach was demonstrated via a combination of spectroscopic techniques, which allowed us to gain a better understanding of the packing of the helicene moieties grafted at the surface. For the first time, thiahelicene triggered release was demonstrated: collected spectroscopic evidence supported the helicene release in mild acidic conditions. Release kinetics tests showed a clear pH dependence, also confirmed by preliminary *in vitro* cell viability tests on two tumour cell lines with different extracellular pH values.

Therefore, these systems proved promising candidates for the triggered release of this cytotoxic compound for potential therapeutic applications. Future developments will take advantage of the intrinsic surface duality of halloysite nanotubes to achieve selective modification of their inner lumen and outer layer to perform different tasks. In this perspective, this may open new paths towards the development of tailored drug delivery systems for theranostics.

Conflicts of interest

There are no conflicts to declare.

Acknowledgements

The authors wish to thank Dr Kevin C. Prince (ELETTRA Synchrotron) for precious advice and comments. The authors thank iMinerals Inc. for providing complimentary samples. The Elettra

Synchrotron Light Laboratory at Trieste (Italy) is acknowledged for beam-time provision. S.C. thanks Università degli Studi di Milano (Piano di Sostegno alla Ricerca 2018 - Linea 2 Azione A - Giovani Ricercatori) for financial support.

Notes and references

1. Y. Shen, and C.-F. Chen, *Chem. Rev.*, 2012, **112**, 1463–1535.
2. G. Song, and J. Ren, *Chem. Commun.*, 2010, **46**, 7283.
3. Y. Xu, Y. X. Zhang, H. Sugiyama, T. Umano, H. Osuga, and K. Tanaka, *J. Am. Chem. Soc.*, 2004, **126**, 6566–6567.
4. S. Sakunkaewkasem, A. Petdum, W. Panchan, J. Sirirak, A. Charoenpanich, T. Sooksimuang, and N. Wanichacheva, *ACS Sensors*, 2018, **3**, 1016–1023.
5. K. Shinohara, Y. Sannohe, S. Kaieda, K. Tanaka, H. Osuga, H. Tahara, Y. Xu, T. Kawase, T. Bando, and H. Sugiyama, *J. Am. Chem. Soc.*, 2010, **132**, 3778–3782.
6. Z. An, and M. Yamaguchi, *Chem. Commun.*, 2012, **48**, 7383.
7. D. Balogh, Z. Zhang, A. Cecconello, J. Vavra, L. Severa, F. Teply, and I. Willner, *Nano Lett.*, 2012, **12**, 5835–5839.
8. S. Cauteruccio, C. Bartoli, C. Carrara, D. Dova, C. Errico, G. Ciampi, D. Dinucci, E. Licandro, and F. Chiellini, *Chempluschem*, 2015, **80**, 490–493.
9. M. Li, L.-H. Feng, H.-Y. Lu, S. Wang, and C.-F. Chen, *Adv. Funct. Mater.*, 2014, **24**, 4405–4412.
10. A. Babič, S. Pascal, R. Duwald, D. Moreau, J. Lacour, and E. Allémann, *Adv. Funct. Mater.*, 2017, **27**, 1701839.
11. Y. Lvov, W. Wang, L. Zhang, and R. Fakhrullin, *Adv. Mater.*, 2016, **28**, 1227–1250.
12. P. Yuan, D. Tan, and F. Annabi-Bergaya, *Appl. Clay Sci.*, 2015, **112**–**113**, 75–93.
13. T. Taroni, D. Meroni, K. Fidecka, D. Maggioni, M. Longhi, and S. Ardizzone, *Appl. Surf. Sci.*, 2019, **486**, 466–473.
14. W. O. Yah, A. Takahara, and Y. M. Lvov, *J. Am. Chem. Soc.*, 2012, **134**, 1853–1859.
15. J. Yang, Y. Wu, Y. Shen, C. Zhou, Y. F. Li, R. R. He, and M. Liu, *ACS Appl. Mater. Interfaces*, 2016, **8**, 26578–26590.
16. E. Licandro, C. Rigamonti, M. Ticozzelli, M. Monteforte, C. Baldoli, C. Giannini, and S. Maiorana, *Synthesis (Stuttg).*, 2006, **2006**, 3670–3678.
17. S. R. MacEwan, D. J. Callahan, and A. Chilkoti, *Nanomedicine*, 2010, **5**, 793–806.
18. Y. Kato, S. Ozawa, C. Miyamoto, Y. Maehata, A. Suzuki, T. Maeda, and Y. Baba, *Cancer Cell Int.*, 2013, **13**, 89.
19. M. Massaro, R. Amorati, G. Cavallaro, S. Guernelli, G. Lazzara, S. Milioto, R. Noto, P. Poma, and S.

Riela, *Colloids Surfaces B Biointerfaces*, 2016, **140**, 505–513.

20. D. Meroni, L. Lo Presti, G. Di Liberto, M. Ceotto, R. G. Acres, K. C. Prince, R. Bellani, G. Soliveri, and S. Ardizzone, *J. Phys. Chem. C*, 2017, **121**, 430–440.
21. G. Soliveri, V. Pifferi, R. Annunziata, L. Rimoldi, V. Aina, G. Cerrato, L. Falciola, G. Cappelletti, and D. Meroni, *J. Phys. Chem. C*, 2015, **119**, 15390–15400.
22. P. M. Dietrich, C. Streeck, S. Glamsch, C. Ehlert, A. Lippitz, A. Nutsch, N. Kulak, B. Beckhoff, and W. E. S. Unger, *Anal. Chem.*, 2015, **87**, 10117–10124.
23. N. Rathor, and S. Panda, *Mater. Sci. Eng. C*, 2009, **29**, 2340–2345.
24. A. Bossi, L. Falciola, C. Graiff, S. Maiorana, C. Rigamonti, A. Tiripicchio, E. Licandro, and P. R. Mussini, *Electrochim. Acta*, 2009, **54**, 5083–5097.
25. Y. Zhang, X. He, J. Ouyang, and H. Yang, *Sci. Rep.*, 2013, **3**, 2948.
26. K. M. Ng, Y. T. R. Lau, C. M. Chan, L. T. Weng, and J. Wu, *Surf. Interface Anal.*, 2011, **43**, 795–802.
27. R. G. Acres, A. V. Ellis, J. Alvino, C. E. Lenahan, D. A. Khodakov, G. F. Metha, and G. G. Andersson, *J. Phys. Chem. C*, 2012, **116**, 6289–6297.
28. Halloysite dataset, http://rruff.geo.arizona.edu/AMS/result.php?mineral=Halloysite, (accessed October 2019).
29. J. Noh, E. Ito, K. Nakajima, J. Kim, H. Lee, and M. Hara, *J. Phys. Chem. B*, 2002, **106**, 7139–7141.
30. M. Kehrer, J. Duchoslav, A. Hinterreiter, M. Cobet, A. Mehic, T. Stehrer, and D. Stifter, *Plasma Process. Polym.*, 2019, **16**, 1800160.
31. N. Graf, E. Yegen, T. Gross, A. Lippitz, W. Weigel, S. Krakert, A. Terfort, and W. E. S. Unger, *Surf. Sci.*, 2009, **603**, 2849–2860.
32. G. M. Su, S. N. Patel, C. D. Pemmaraju, D. Prendergast, and M. L. Chabinyc, *J. Phys. Chem. C*, 2017, **121**, 9142–9152.
33. Q. Peng, K. Efimenko, J. Genzer, and G. N. Parsons, *Langmuir*, 2012, **28**, 10464–10470.
34. S. Maiorana, A. Papagni, E. Licandro, R. Annunziata, P. Paravidino, D. Perdicchia, C. Giannini, M. Bencini, K. Clays, and A. Persoons, *Tetrahedron*, 2003, **59**, 6481–6488.